COMPARATIVE ANALYSIS OF NUMERICAL SIMULATIONS OF BLOOD FLOW THROUGH THE SEGMENT OF AN ARTERY IN THE PRESENCE OF STENOSIS

Fozia Shaikh[1], Asif Ali Shaikh[1,2], Evren Hincal[2], Sania Qureshi[1,2,3]

[1] *Department of Basic Sciences and Related Studies, Mehran University of Engineering and Technology, Sindh, Pakistan*
[2] *Department of Mathematics, Near East University Mersin, Turkey*
[3] *Department of Computer Science and Mathematics, Lebanese American University Beirut, Lebanon*
fozia.shaikh@faculty.muet.edu.pk, asif.shaikh@faculty.muet.edu.pk, evren.hincal@neu.edu.tr sania.shahid@lau.edu.lb

Abstract. A mathematical model is developed to study the characteristics of blood flowing through an arterial segment in the presence of a single and a couple of stenoses. The governing equations accompanied by an appropriate choice of initial and boundary conditions are solved numerically by Taylor Galerkin's time-stepping equation, and the numerical stability is checked. The pressure, velocity, and stream functions have been solved by Cholesky's method. Furthermore, an in-depth study of the flow pattern reveals the separation of Reynolds number for the 30 and 50% blockage of single stenosis and 30% blockage of multi-stenosis. The present results predict the excess pressure drop across the stenosis site than it does for the inlet of the artery with single and multiple stenosis and the increase in the velocity is observed at the center of the artery.

1. Introduction

Atherosclerosis is currently the primary health concern that contributes to the narrowing of the artery lumen in emerging and impoverished nations. Consequently, the establishment of stenosis, which is abnormal growth due to cholesterol and fats, disrupts the normal flow of blood. This causes hypertension, stroke, and some cardiovascular diseases, which are the major causes of death, particularly in emerging countries. Thus, it is very important to study the different factors such as pressure drop, velocity, wall shear stress, etc. for the natural movement of blood and behavior of stenosed arteries and the advance of the pathological condition [1]. Investigation of modeling of the blood flow through segments of an artery with multiple stenoses

is very arduous nowadays. The main components on which the accuracy of the model depends are the appropriate numerical scheme, model's geometry, and boundary conditions. Research investigators keep their attention on blood flow through arteries with mule stenosis. The behavior of the flow of blood as a nanofluid through a stenosed artery was studied by Hussain et al. [2]. They used similarity transformation for the solution of a differential equation. Investigation of blood flow in the branched artery with the blockage of 20, 50, and 80% was done in [3] and concluded that in 80% blockage, the shear rate is high in the re-circulation area with an increasing Reynolds number. One-dimensional non-Newtonian fluid in the presence of multiple stenoses in an artery was investigated [4]. The artery they considered during the investigation was about 45 mm in length, 0.45 mm in radius, and 15 mm in length, and concluded that the ratio of resistance becomes approximately one with decreasing viscosity and increasing stress. Using an analytical technique, a thorough single-phase mathematical analysis of blood nanofluid passing through an inclined stenosed artery in the vicinity of a magnetic field was performed [5]. The findings showed that a magnetic field decreased the blood nanofluid's velocity through arteries. With the assistance of the finite difference method, a nonlinear blood flow model under the influence of periodic body acceleration through several stenosed arteries was examined [6]. The outcomes demonstrated that the wall shear stress increases as the Reynolds number increases. The Bernstein polynomial approximation method is used to investigate the Newtonian gold-blood nanofluid flowing through a stenosed artery in the presence of a magnetic field and concluded with the findings that as the particle concentration increases in the presence of the magnetic field, the temperature and wall shearing stress of the nanofluid increase, whereas the velocity decreases [7]. A theoretical study was conducted on ternary hybrid nanoparticles using homotopy perturbation methodology in an inclined catheterized artery with multiple stenoses and wall slip [8].

An axially non-symmetrical stenosed artery with a flexible tube, and a two-layer model of blood, was under study [9]. Srivastava proposed the size of the tube must not be more than 50% of the artery. An investigation was done on the irregular stenosis of a 3D computational model using finite element volume [10]. Homotopy perturbation was used to examine the impact of hybrid nanoparticles (Cu–TiO$_2$) on peristaltic blood flow patterns in a nonuniform cylindrical annulus with wall slip inside an external induced magnetic field [11]. According to Gupta's findings, the oscillations in wall shear stresses are stronger in cases of irregular stenosis for Re = 130-540. Under the influence of a magnetic field tapered artery was under investigation [12]. A homotopy perturbation method was used to examine the effects of a magnetic field, thermophoresis, and Brownian force on blood nanoparticles in an inclined coaxial tube [13]. Neetu resulted that stress decreasing very fast downstream and is very high near the stenosis. Furthermore, the results showed that with an increase in the Hartmann number, and a decrease in the flow rate. The non-Newtonian Casson blood model in the stenosed artery was investigated [14] with slip condition and concluded that slip velocity increases, whereas shear stress and yield stress reduce in

a radial direction. Bioheat transfer in biological tissue and analysis of blood temperature along the artery and vein was taken into account [15]. The Reciprocity Boundary Element Method (MRBEM) and finite difference method were applied for solving the Pennes equation. Researchers have employed different numerical techniques for solving the differential models developed from nonlinear fluids. A numerical scheme using Riemann-Liouville fractional operator, Caputo fractional operators as well as Atangana-Baleanu-Caputo can also be used to solve the differential equations obtained from nonlinear fluid models [16–21].

2. Problem formulation

Steady, Newtonian form of the blood with constant density partaking symmetric stenosis specified at single and multi-position in the segment of an artery are considered in this paper. Assuming that R(x) is the radius of the stenotic region and R is the radius of the non-stenotic region. The Navier-Stokes equation governs the fluid model and is drawn up in the cylindrical coordinate system (r, θ, x), where (r, θ) are the coordinates in the radial and circumferential direction, and the x-axis represents the coordinate along the axis of an artery as illustrated in Figure 1. The flow is induced by an axial pressure gradient by neglecting the gravitational effects.
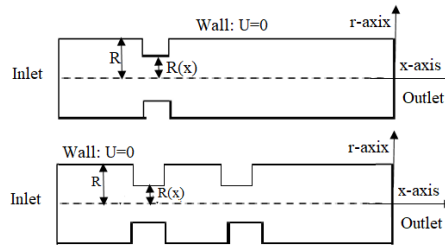
Fig. 1. A graphical illustration of the physical model

3. Governing equations

Governing equations govern the Newtonian fluid flow, and are described as continuity equation and momentum equation and are depicted as follows:

$$\nabla . u = 0, \tag{1}$$

$$\rho \left(\frac{\partial u}{\partial t} + u . \nabla u \right) = -\nabla P + \rho . F + \nabla . \tau, \tag{2}$$

where velocity is u, density of the fluid is ρ, P is the pressure, and F is the body force. Stress tensor τ for Newtonian fluid, is stated as $\tau = 2\mu_1 D$, where D is the rate of deformation tensor and velocity gradient L, is defined as:

$$D = \frac{L + L^t}{2}, \quad \text{where} \quad L^t = \nabla u. \tag{3}$$

Describing the non-dimensional variables for velocity, distance, and shear stress respectively as,

$$u^* = \frac{u}{U}, \quad x^* = \frac{x}{L}, \quad P^* = \frac{L}{\mu_0 U} P, \quad \tau^* = \frac{L}{\mu_0 U} \tau, \quad \text{and} \quad \mu^* = \frac{\mu_1}{\mu_0}. \tag{4}$$

Discarding the '*' notation, equations (1) and (2) can be rewritten as (5) and (6) shown below:

$$\frac{2Re}{\Delta t}(u^{n+1} - u^n) = (\nabla.(2\mu D) - Re u.\nabla u)^n - \nabla p^{n+1}, \tag{5}$$

$$\nabla.u^{n+1} = 0. \tag{6}$$

where *Re* is the non-dimensional number known as the Reynolds number which portrays the behavior of blood and is defined as:

$$Re = \frac{\rho u L}{\mu}. \tag{7}$$

4. Numerical simulations

Numerical simulation techniques such as the finite element method (FEM), finite volume method (FVM), and computational fluid dynamics (CFD) have proven to be valuable tools in the study of blood flow through the segment of an artery in the presence of stenosis. These techniques have enabled researchers to model complex geometries, accurately simulate blood flow parameters, and investigate the effects of stenosis on blood flow. From a wide range of numerical schemes, Semi-implicit Taylor-Galerkin/Pressure-correction is used for discretization in this paper. The main goal of the Taylor-Galerkin scheme is to provide a time-stepping system that is effective and extremely accurate in capturing both transient and steady-state solutions to fluid flow challenges. The approach was first put forth by Chorin [22], and it was afterward improved by Fortin and Esselaoui [23]. It splits the pressure fields and velocity fields. For non-Newtonian fluids, however, the approach has been improved numerically in both semi-implicit and fully-implicit forms. The semi-implicit technique has shown to be numerically correct and computationally effective for flows that are diffusion dominant, giving it a reliable option for particular challenges. The semi-implicit type of the TGCP algorithm is used in the proposed study. Velocity and pressure regions are calculated then approximately as: $u = \sum_i u^i(t)\phi_i(x)$ and $p = \sum_j p^j(t)\psi_j(x).$

Here $\phi_i(x)$ is the parabolic shape function for the velocity and for pressure $\psi_j(x)$ is the linear shape function. The corresponding finite element method, semi-implicit Taylor-Galerkin/Pressure-correction form of equations may then be articulated in matrix form as:

$$M_{ij} = \int_{\Omega} \phi_i \phi_j d\Omega, \tag{8}$$

$$N(U)_{ij} = \int \phi_i \phi_j U \nabla \phi_j d\Omega, \tag{9}$$

$$((L_k)_{ij}) = \int_{\Omega} \psi_i \frac{\partial \phi_j}{\partial x_k} d\Omega, \tag{10}$$

$$K_{ij} = \int_{\Omega} \nabla \psi_i \psi_j d\Omega, \tag{11}$$

$$S_{ij} = \int_{\Omega} \nabla \phi_i \phi_j d\Omega. \tag{12}$$

where M, S, $N(U)$, L, K are consistent mass matrix, diffusive matrix, convection matrix, pressure-gradient matrix, and pressure-stiffness matrix, respectively. Choleskey's method is then applied to the matrix equation for a solution.

5. Results and discussions

This section concentrates on investigated numerical results. The simulated model is expounding the results of a symmetric single stenosed segment of an artery for the blockage of 30 and 50%, and a multi-stenosed segment of an artery blocked 30% in this piece of work. Results of important parameters such as velocity profiles, contour plots of pressure profiles, and streamline functions of the blocked artery are trotting out with different Reynolds numbers (say, $Re = 10$, $Re = 400$, and $Re = 1000$) which is the important factor of this modeling that highlights the flow rate at inlet, outlet, and near the stenosis of a blocked artery. Meshes with different blockage percentages of single and multi-stenosed arteries were generated using IDEAS software, and the numerical solution is obtained using FORTRAN programming language. The mesh of the symmetric artery with 30% blockage has 1680 elements and 3523 nodes, whereas the mesh of 50% blockage has 11277 elements and 5480 nodes and is used for the investigation of blood flow due to various blockages. Similarly, the mesh of the multi-symmetric artery with blockage 30% has 8928 elements and 4699 nodes. The results converge up to the 10^{-6}.

Fully developed velocity vectors for both 30% and 50% blockage in a single symmetric stenosed artery are illustrated in Figure 2a-2b, whereas a multi-stenosed artery

for 30% blockage is depicted in Figure 2c. It can be noticed that the flow is laminar, the velocity profile is parabolic, and a similar trend is observed at the outlet for both the cases of single and multi blockage 30% which guarantees the stability of the numerical scheme. Additionally, a parabolic trend of velocity is noticed at the inlet and outlet for 50% blockage, however, it needs more force to flow near the blockage.

(a) *Blockage   30%*   (b) *Blockage   50%*
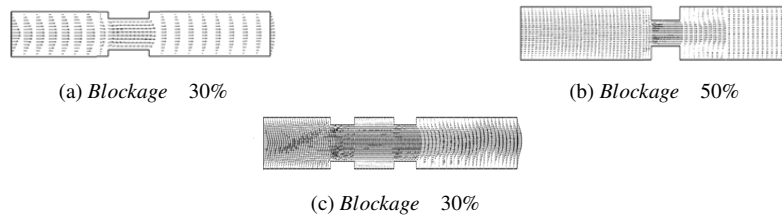
(c) *Blockage   30%*

Fig. 2. Velocity vectors for single and multi-stenosed artery

Figure 3a-3c illustrates the velocity contours with different Reynolds number sand such as $Re = 10$, $Re = 400$, and $Re = 1000$ for blockage of 30% respectively, and can be noticed here that the flow is speedy with increasing Reynolds number. Figure 3a describes a slight increase in the velocity at the inlet and at the stenosis site and it decreases as blood passes the stenosis site. Figure 3b-3c demonstrates an increase in the velocity of the blood at the center of the artery for both $Re = 400$ and $Re = 1000$.

(a) $Re = 10$ (b) $Re = 400$

(c) $Re = 1000$
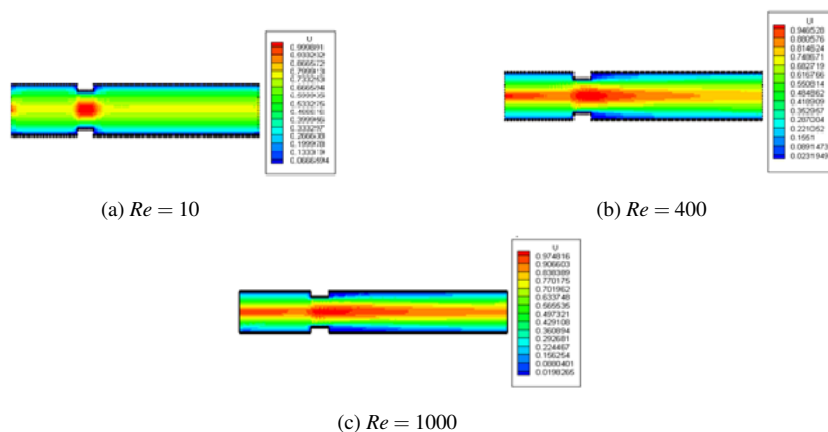
Fig. 3. Velocity contours for 30% blockage

Figure 4a-4c displays the blockage of 50% with various Reynolds numbers respectively. Velocity seems to increase at the stenosis site with an increasing Reynolds number, and blood is absent near the end of stenosis in all the cases. It can further be noticed that with an increasing Reynolds number, blood shoots at the stenosis site with more speed. Comparatively, the blood flow is quick initially at the inlet as well as at the stenosis site with an increasing Reynolds number for 30% blockage whereas fluid shoots out with more force at the stenosis region for blockage of 50%, and maximum velocity is observed at the center of stenosis. In addition, a slight disturbance,

and re-circulation are seen at the exit of the stenosis site in 50% blockage, which causes increases in the stenosis at that region.

(a) $Re = 10$
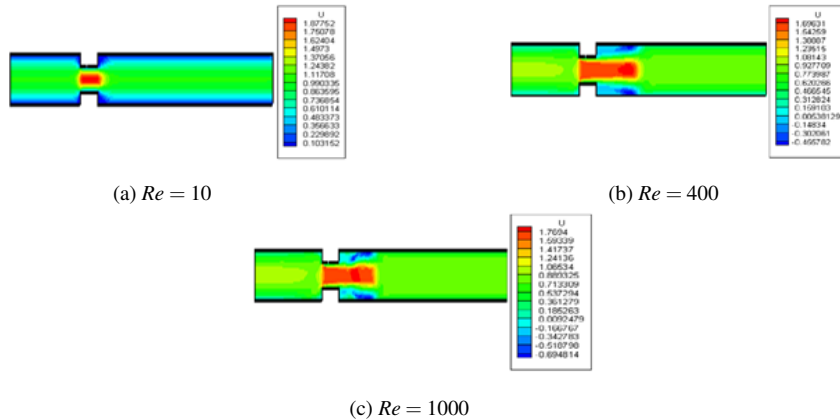
(b) $Re = 400$

(c) $Re = 1000$

Fig. 4. Velocity contours for 50% blockage

Figure 5a-5c depicted the velocity contours of 30% blockage of the muli-stenosed artery with various Reynolds numbers i.e. $Re = 10$, $Re = 400$, and $Re = 1000$.

(a) $Re = 10$
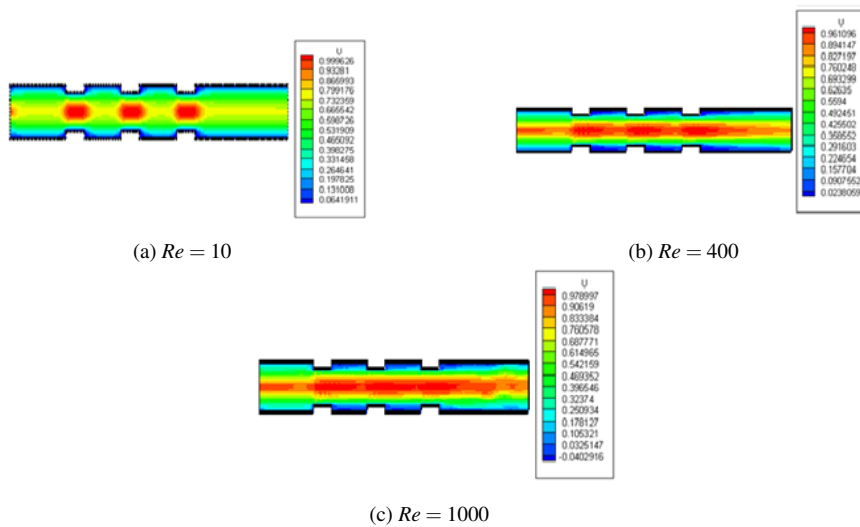
(b) $Re = 400$

(c) $Re = 1000$

Fig. 5. Velocity contours for 30% blockage

Figure 5a describes that peak velocity is at the inlet as well as at the center of each stenosis site and decreases as the blood passes the stenosis site, and a similar trend is seen for $Re = 400$ and $Re = 1000$. However, the flow is speedy and shoots out with force at the center from the inlet to the outlet in Figure 5b-5c. Furthermore, the flow seems absent at the upper and lower walls of the artery. A comparative study of single and multi-stenosis demonstrates that maximum velocity is at the center with

an increasing Reynolds number for both 30% and 50% blockage. The blood flow is fast at the stenosis site, and reversal flow is seen right after stenosis in 50% blockage that causes an increase in the size of the stenosis in a single stenosed artery and more severe in 30% blockage multi-stenosed artery.

When an artery becomes blocked, the part of the body supplying blood to that artery will suffer a lack of oxygen, and energy, and die. When the ruptured blood vessel is inside the brain, it results in a stroke, while it causes a heart attack when it is inside the heart. Thus, it is very important to study artery pressure distribution.

(a) $Re = 10$

(b) $Re = 400$

(c) $Re = 1000$
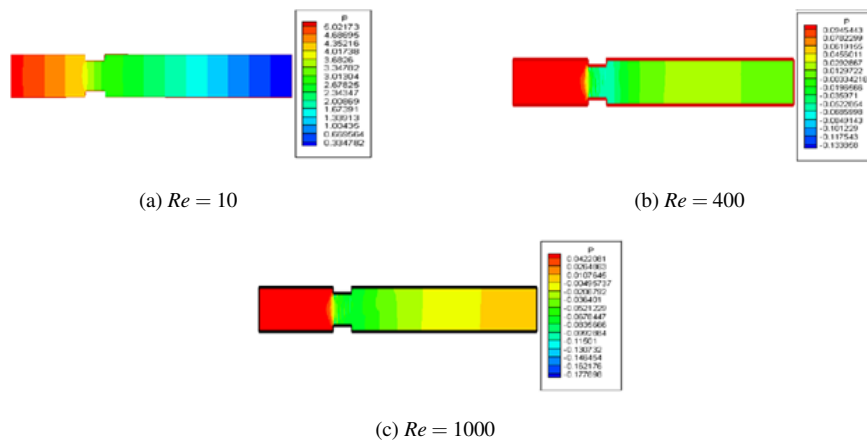
Fig. 6. Pressure contours for single stenosis 30% blockage

(a) $Re = 10$

(b) $Re = 400$

(c) $Re = 1000$
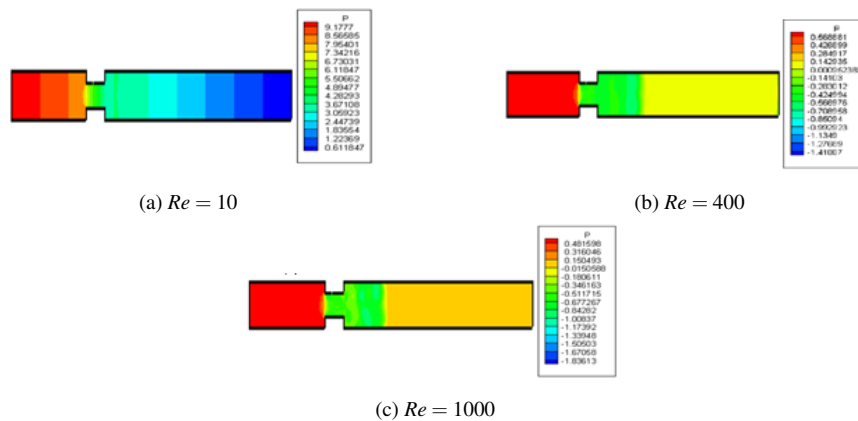
Fig. 7. Pressure contours for single stenosis 50% blockage

Pressure contours are depicted in Figure 6a-6c for forenamed Reynolds numbers for 30% blockage single stenosis. It can be noticed that the high pressure is at the inlet for a low Reynolds number, and it drops gradually as the blood travels toward the stenosis and completely vanishes at the outlet. It can further be noted here that for an increasing Reynolds number, pressure increases with more force, and it suddenly

drops as the blood reaches the stenosis region. A similar trend is observed for the aforementioned Reynolds numbers, with blockage of 50%, however, a high force is required to flow the blood in a narrow region (Fig. 7a-7c).

Figure 8a-8c portrays the pressure contour for the blockage of 30% multi-stenosed artery. It demonstrates the drop in the pressure gradually when blood is passing the stenosis region. Moreover, the absence of blood flow at the walls of each stenosis exit, and the change in the flow rate of blood cause a transition in the pressure and increase the size of the stenosis.

(a) $Re = 10$ (b) $Re = 400$

(c) $Re = 1000$
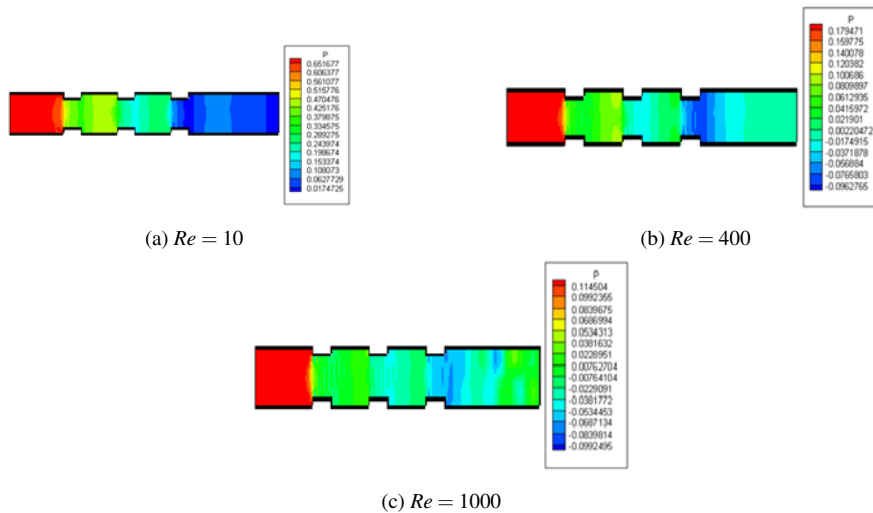
Fig. 8. Pressure contours for multi-stenosis 30% blockage

(a) $Re = 10$ (b) $Re = 400$

(c) $Re = 1000$
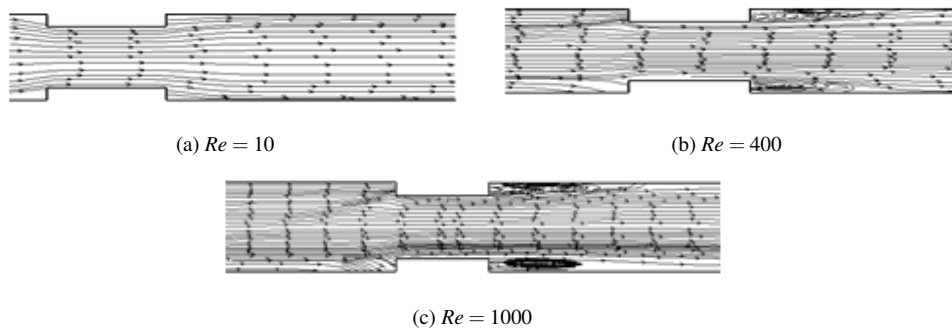
Fig. 9. Streamline function for 30% blockage for different Reynolds numbers

A streamline is a set of points that are tangent to the instantaneous velocity vector everywhere. These lines are helpful for observing the separation zone (vortex) formed inside the artery near the wall. Thus, these separation regions are pathologically significant since they prolong the residence time of blood constituents that may cause

blood clots or thrombosis. Figure 9 renders the view of streamlines of flow in the different locations for three aforementioned Reynolds numbers of 30% blockage. Near the axis, all streamlines go in a straight line, but as they approach the stenotic artery's wall, their trajectory becomes increasingly disordered (Fig. 9a). It is noteworthy here (Fig. 9b-9c) that while some flow lines pass through the constricted region right after the mainstream, others are lured to the stenotic wall upstream by the emergence of circulation zones with increasing Reynolds numbers. Recirculation is severe at the exit of the stenosis region for the Reynolds number for $Re = 1000$, and this causes an increase in the size of the stenosis at that region.

The streamlined distribution for the blockage of 50% is plotted in Figure 10a--10c. With increasing Reynolds numbers, flow lines seem smooth along with the flow field, however, the discontinuity in the flow is observed at the exit of the segment of an artery for a small Reynolds number. Since the blood is passing through the narrow space with high force, discontinuity in the streamlines is therefore clear at the stenosis site with large size vortices at the exit of the stenosis region. The severe disruption in the streamlines is visible at the entrance of the narrow region, and recirculation of the flow appears at the exit of the restrained for increasing Reynolds numbers which is evidence of the harshness of the vortex and the wake enlargement at that region.

(a) $Re = 10$ (b) $Re = 400$

(c) $Re = 1000$
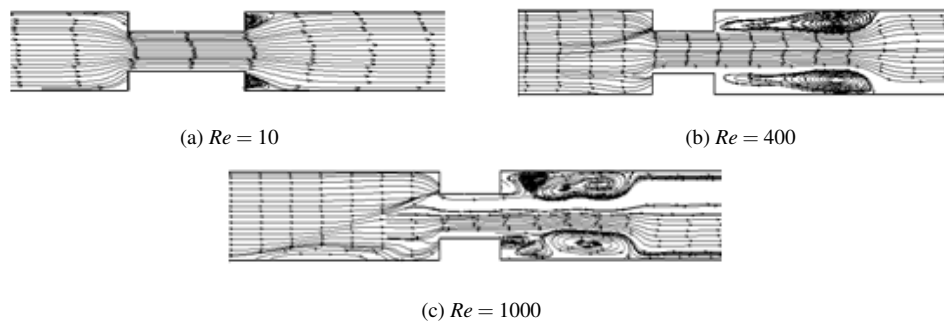
Fig. 10. Streamline function for 50% blockage for different Reynolds numbers

The streamlines simulation of multi-stenosis of blockage 30% is shown in Figure 11a-11c. It is interesting to observe in Figures that several flow lines are striking the stenotic wall and then the re-circulation zone forms near the upstream and downstream exit of the stenosis site. The severity of the vorticity increases at the exit of each constraint with an increasing Reynolds number. Comparatively, that prompts expansion of plaque in a 50% blocked artery is more severe in Reynolds numbers 400 and 1000, as well as in a 30% muti-stenosed artery. Flow turbulence properties are generated in a narrow artery of 50% blockage with single stenosis rather than high intensity in a 30% multi-stenosed artery.

(a) $Re = 10$

(b) $Re = 400$

(c) $Re = 1000$
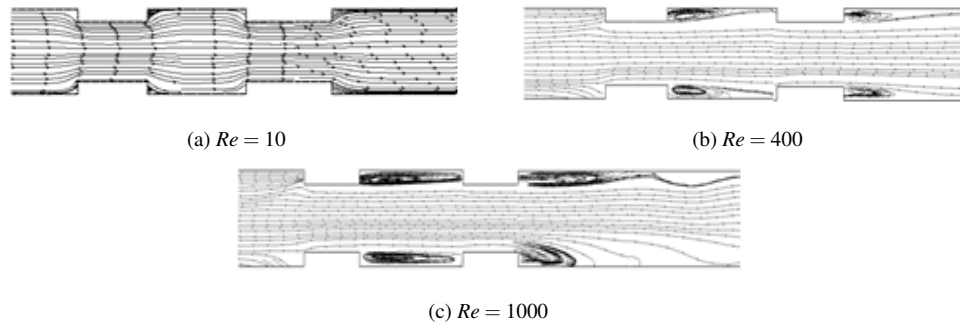
Fig. 11. Streamline function of multi-stenosis artery for 30% blockage for different Reynolds numbers

6. Conclusion

We investigated the blood flow through the single and multi-stenosed segments of arteries. Our investigation depicts that flow changes its pattern from laminar to turbulent in single and multi-stenosed arteries with 30% and 50% blockage. As the Reynolds number rises, the inlet center velocity increases noticeably. Maximum pressure is likewise seen near the artery's inlet, and it lowers gradually as blood moves through the stenosis area. Furthermore, from the above figures, in this paper, a comparative study reveals that flow is quite laminar in 30% blockage single stenosis. However, in 50% blockage, with increasing Reynolds numbers reversal of flow appears due to a pressure drop that decelerates the flow and re-circulation appears, causing increases in the length of the vortex at that region. In addition, flow deceleration at each stenosis exit with increasing Reynolds numbers also drops pressure fast and vortex grows with more strength in 30% blockage multi-stenosed artery that may transform this reversal flow into lumps and this lump may be the cause of further disease normally called atherosclerosis.

References

[1] Chatterjee, A., Changdar, S., & De, S. (2020). Study of nanoparticle as a drug carrier through stenosed arteries using Bernstein polynomials. *International Journal for Computational Methods in Engineering Science and Mechanics*, *21*(5), 243-251.

[2] Hussain, A., Sarwar, L., Rehman, A., Al Mdallal, Q., Almaliki, A.H., & El-Shafay, A.S. (2022). Mathematical analysis of hybrid mediated blood flow in stenosis narrow arteries. *Scientific Reports*, *12*(1), 12704.

[3] Shaikh, A., & Chandio, M. (2014). Computation of blood flow separation and reattachment length on Stenosed artery using Finite Element Method. *Sindh University Research Journal – SURJ (Science Series)*, *46*(4).

[4] Kumar, H., & Chandel, R. (2014). A non-Newtonian arterial blood flow model through multiple stenosis. *International Journal of Latest Research in Science and Technology*, *3*(3), 116-121.

[5] Changdar, S., & De, S. (2017). Analytical solution of mathematical model of magnetohydro-dynamic blood nanofluid flowing through an inclined multiple stenosed artery. *Journal of Nanofluids*, *6*(6), 1198-1205.

[6] Changdar, S., & De, S. (2015). Numerical simulation of nonlinear pulsatile Newtonian blood flow through a multiple stenosed artery. *International Scholarly Research Notices*, *2015*, 628605.

[7] Changdar, S., & De, S. (2019). Analytical investigation of nanoparticle as a drug carrier sus-pended in a MHD blood flowing through an irregular shape stenosed artery. *Iranian Journal of Science and Technology, Transactions A: Science*, *43*, 1259-1272.

[8] Dolui, S., Bhaumik, B., & De, S. (2023). Combined effect of induced magnetic field and thermal radiation on ternary hybrid nanofluid flow through an inclined catheterized artery with multiple stenosis. *Chemical Physics Letters*, *811*, 140209.

[9] Srivastav, K. (2015). Two-Layered Model of blood flow through arterial catheterization with non-symmetric constriction. *Journal of Computation in Biosciences and Engineering*, *2*(2), 1-8.

[10] Gupta, A.K., & Agrawal, S.P. (2015). Computational modeling and analysis of the hydrodynamic parameters of blood through stenotic artery. *Procedia Computer Science*, *57*, 403-410.

[11] Srivastava, N. (2014). Analysis of flow characteristics of the blood flowing through an inclined tapered porous artery with mild stenosis under the influence of an inclined magnetic field. *Journal of Biophysics*, *2014*, 797142.

[12] Dolui, S., Bhaumik, B., De, S., & Changdar, S. (2023). Effect of a variable magnetic field on peristaltic slip flow of blood based hybrid nanofluid through a non-uniform annular channel. *Journal of Mechanics in Medicine and Biology*, *23*, 2250070.

[13] Bhaumik, B., Changdar, S., & De, S. (2022). Combined impact of Brownian motion and thermo-phoresis on nanoparticle distribution in peristaltic nanofluid flow in an asymmetric channel. *International Journal of Ambient Energy*, *43*(1), 5064-5075.

[14] Gaur, M., & Gupta, M.K. (2014). A Casson fluid model for the steady flow through a stenosed blood vessel. *British Journal of Mathematics and Computer Sciences*, *4*(11), 1629-1641.

[15] Majchrzak, E., & Tarasek, D. (2011). Numerical analysis of heat transfer in countercurrent blood flow and biological tissue. *Scientific Research of the Institute of Mathematics and Computer Science*, *10*(2), 143-153.

[16] Shaikh, A.A., & Qureshi, S. (2022). Comparative analysis of Riemann-Liouville, Caputo--Fabrizio, and Atangana-Baleanu integrals. *Journal of Applied Mathematics and Computational Mechanics*, *21*(1), 91-101.

[17] Maayah, B., Moussaoui, A., Bushnaq, S., & Abu Arqub, O. (2022). The multistep Laplace optimized decomposition method for solving fractional-order coronavirus disease model (COVID-19) via the Caputo fractional approach. *Demonstratio Mathematica*, *55*(1), 963-977.

[18] Momani, S., Abu Arqub, O., & Maayah, B. (2020). Piecewise optimal fractional reproducing kernel solution and convergence analysis for the Atangana-Baleanu-Caputo model of the Lienard's equation. *Fractals*, *28*(08), 2040007.

[19] Maayah, B., Arqub, O.A., Alnabulsi, S., & Alsulami, H. (2022). Numerical solutions and geo-metric attractors of a fractional model of the cancer-immune based on the Atangana-Baleanu--Caputo derivative and the reproducing kernel scheme. *Chinese Journal of Physics*, *80*, 463-483.

[20] Arqub, O.A., & Maayah, B. (2022). Adaptive the Dirichlet model of mobile/immobile advection/dispersion in a time-fractional sense with the reproducing kernel computational approach: Formulations and approximations. *International Journal of Modern Physics B*, 2350179.

[21] Arqub, O.A., Hayat, T., & Alhodaly, M. (2021). Reproducing kernel Hilbert pointwise numerical solvability of fractional Sine-Gordon model in time-dependent variable with Dirichlet condition. *Physica Scripta*, *96*(10), 104005.

[22] Chorin, A.J. (1968). Numerical solution of the Navier-Stokes equations. *Mathematics of Computation*, *22*, 104, 745-762.

[23] Fortin, M., & Esselaoui, D. (1987). A finite element procedure for viscoelastic flows. *International Journal for Numerical Methods in Fluids*, *7*, 10, 1035-1052.